Supplement of

A study of the morphology and effective density of externally mixed black carbon aerosols in ambient air using a size-resolved single-particle soot photometer (SP2)

Yunfei Wu et al.

Correspondence to: Yunfei Wu (wuyf@mail.iap.ac.cn) and Renjian Zhang (zrj@mail.iap.ac.cn)

Contents

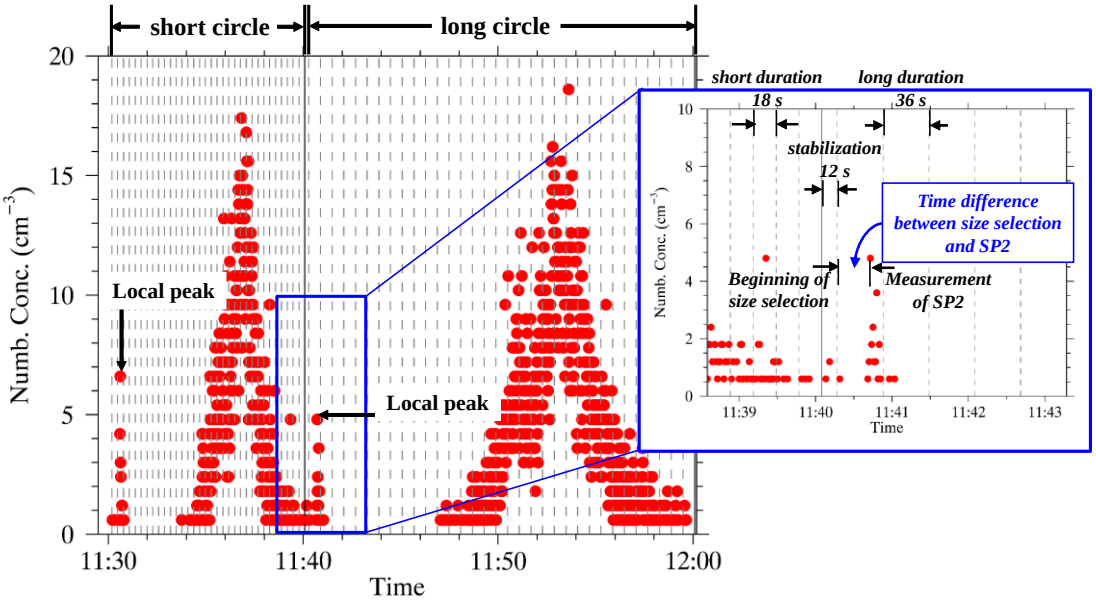

Fig. S1. Temporal variation of the total number concentration of the scattering and incandescence particles detected by the SP2 during a size selection comprising of one short cycle with a duration of 18 s for each size and one long cycle with a duration of 36 s. The local peak at the beginning of each cycle was previously identified to correct the time difference between the DMA size selection and the SP2 measurement.

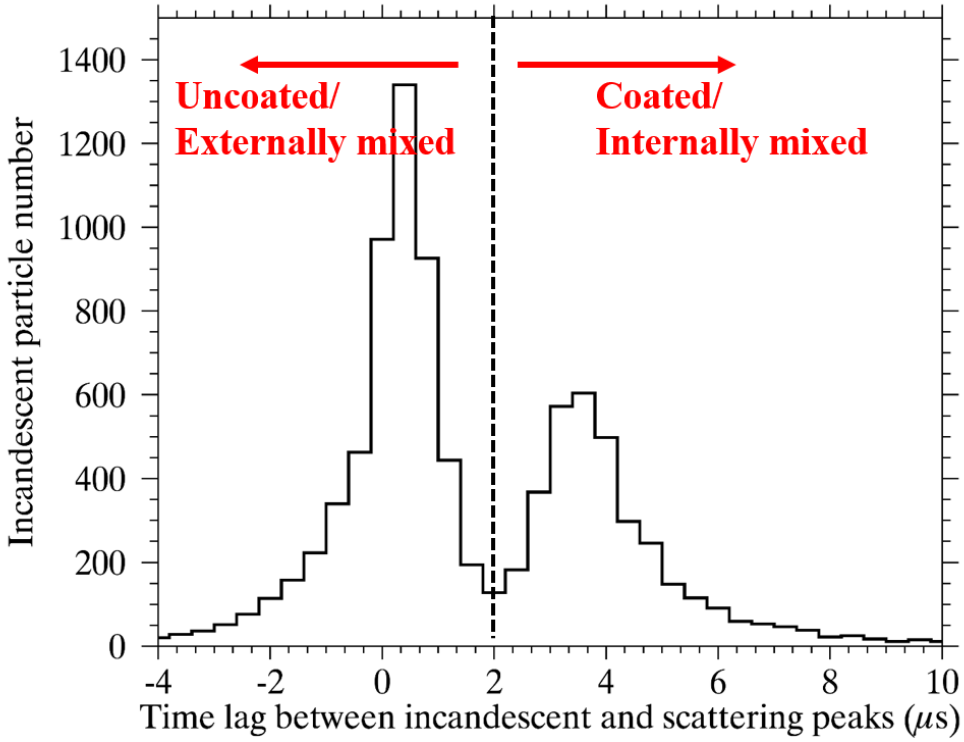

Fig. S2. Frequency distribution of the lag times between the incandescence and scattering peak locations determined using the SP2. A bimodal distribution is found, with the minimum at ~2 μs. The BC-containing particles with a lag time greater than 2 μs were considered to be thickly coated. Otherwise, the BC-containing particles were non/thinly coated.

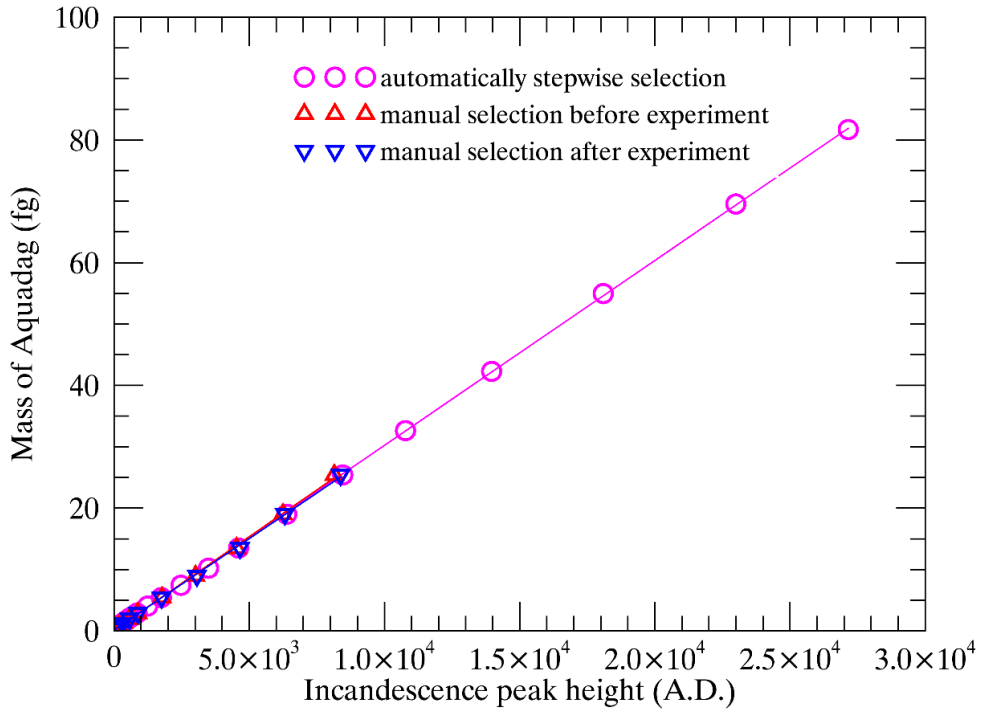

Fig. S3. The calibration curves for the relationship between the SP2-measured incandescence peak height (low gain) and the refractory BC (rBC) mass. The Aquadag particles were used as the representative material of rBC in the calibration. The Aquadag particles with different mobility sizes (d_{mob}=100, 125, 150, 175, 200, 250, 300, 350, 400, 450 nm, respectively) were manually selected by a DMA. The masses of the size-selected Aquadag particles were calculated based on the effective densities (ρ_{eff}) according to the density-mobility relationship provided in Gysel et al. (2011). The manual calibrations were performed both before (on 23 Jan. 2018) and after the campaign (on 10 Feb. 2018). The red up-triangles represent the relationship between the mass of Aquadag and the incandescence peak height during the calibration before campaign. The blue down-triangles represent the calibration after the campaign. It is clear that the SP2 incandescence peak height is proportional to the mass of Aquadag, inferring the linear regression functions as y=0.003048x+0.1058 (R^2=0.9991) for the calibration before campaign and y=0.002972x+0.1713 (R^2=0.9992) for the calibration after campaign. In the functions, y represents the mass of Aquadag, and x represents the incandescence peak height. To examine the detection efficiency of SP2, the size-resolved Aquadag particles were also automatically selected by the DMA in the d_{mob} range of 140–750 nm and then measured using the SP2 and CPC after the campaign. The mass-incandescence relationship derived from this measurement was very close to the manual calibrations. The linear regression function is y=0.003012x+0.1097 (R^2=0.9999). The similar rBC mass calibration curves indicate that the SP2 operated very stably throughout this campaign. Considering that the incandescence signal peaks of Aquadag were ~25% higher than those of the ambient BC particles, the slopes of the calibration equations should multiply by a factor of ~1.33 when converting the measured incandescence signal peaks to the rBC masses for ambient particles.

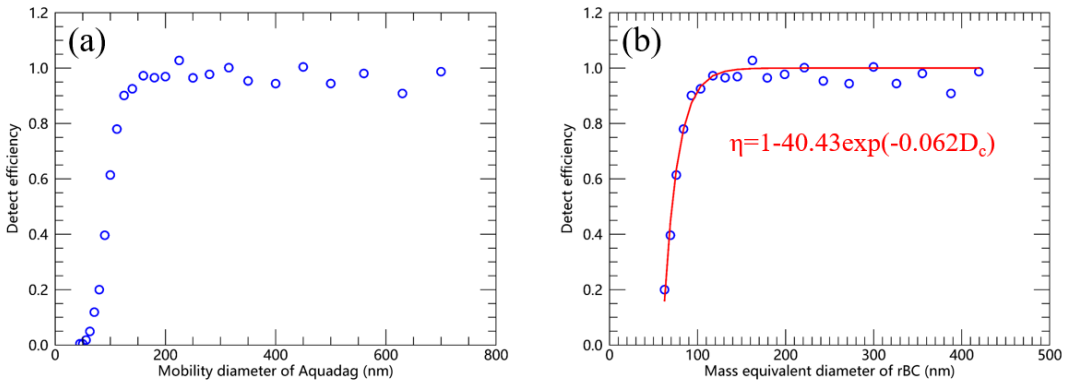

Fig. S4. Detection efficiency of the SP2 as a function of (a) the mobility diameter of Aquadag and (b) the mass-equivalent diameter of rBC. The detection efficiency was calculated as the ratio of the number concentration of particles detected by the SP2 to that parallel measured by the CPC at prescribed mobility sizes. Since the Aquadag particles were generated by an aerosol generator, pure scattering particles should not exist. The particles having detectable incandescence signals were recorded by the SP2. It is clear that adequate detection efficiencies (>~90%) for the SP2 were observed when the d_{mob} of Aquadag was larger than 125 nm. Correspondingly, the mass-equivalent diameter of rBC calculated using the d_{mob} and ρ_{eff} of Aquadag should be larger than ~90 nm to provide adequate detection efficiencies. The relationship between the detection efficiency of the SP2 and the rBC mass can be characterized using an exponential function, as shown in Fig. S4b.

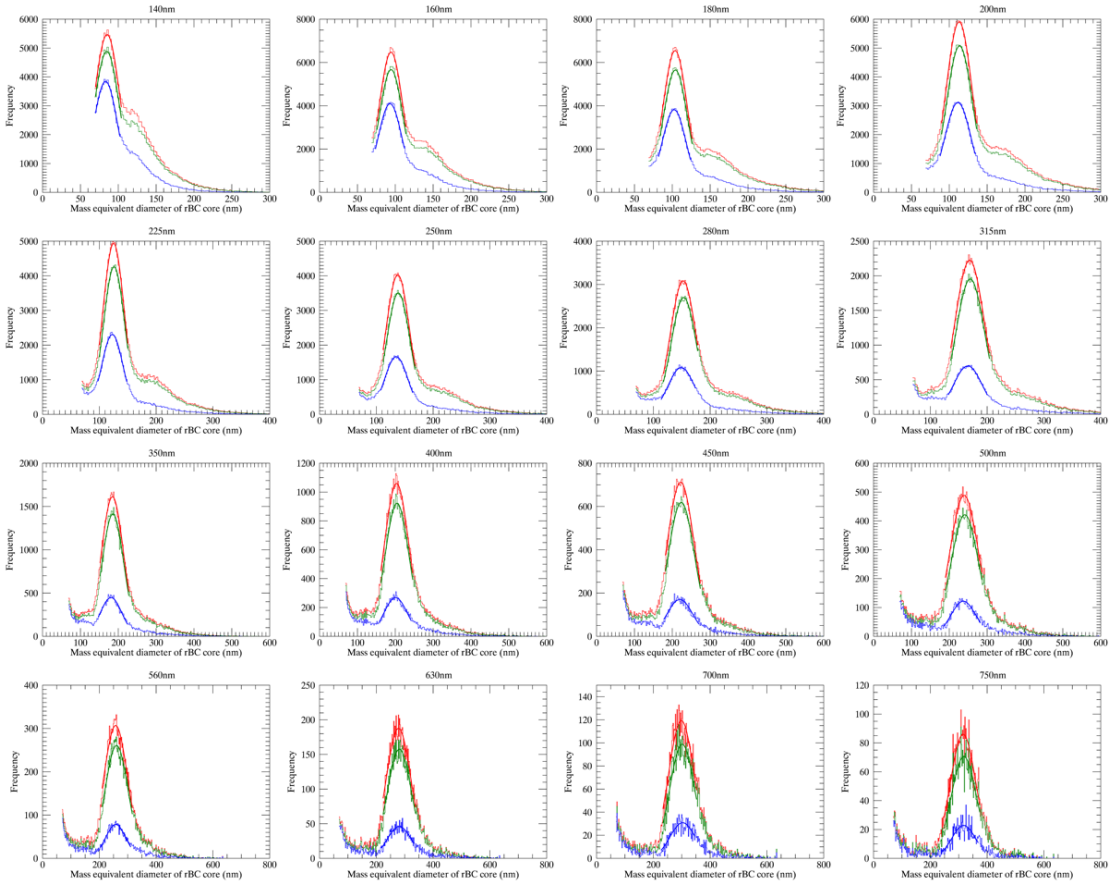

Fig. S5. Frequency distribution of the d_{me} of *ext*BC at 16 prescribed mobility sizes (in the 140–750 nm d_{mob} range) analyzed in the current study. Three thresholds of delay time between the incandescence signal peak and the scattering peak detected by the SP2 were employed to discriminate the *ext*BC particles, e.g., 2.0 μs, 1.2 μs and 0.4 μs. The frequency distributions corresponding to the thresholds are shown in red, green and blue colors, respectively. Reducing the delay time threshold results in a decrease in the data volume used in the statistics, while it seems to have few effects on the peak locations of the distributions. The major peak of the frequency distribution at smaller mobility sizes with a d_{mob}<140 nm is not clear due to the lower limit of the SP2. Thus, these smaller sizes were not discussed in the current study.

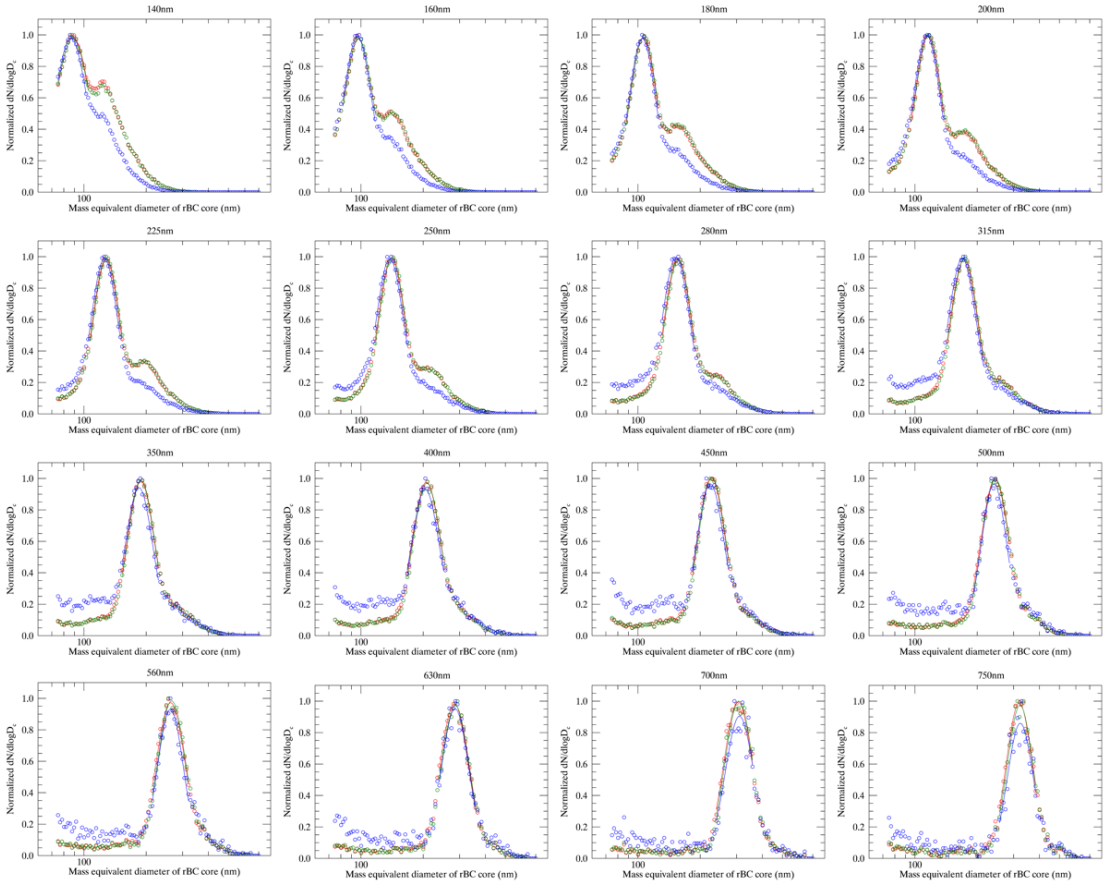

Fig. S6. The same as Fig. S5, but for the normalized number size distribution (dN/dlogD_c). The quantity D_c indicates the mass-equivalent diameter of the rBC core, the same as d_{me} defined above. Compared to Fig. S5, these graphs more clearly show that reducing the time-delay threshold has few effects on the peak d_{me}. The main changes occur at the right tail of the distributions at each mobility size. Reducing the time-delay threshold results in a significant reduction of particles at the right tail of the number size distribution. These particles are likely to be the thinly or even moderately coated BC particles, which were also recognized as *ext*BC using the time-delay approach. Since the peak d_{me} values are needed in the current study, and are considered the typical d_{me} values for the prescribed d_{mob}, these thinly or even moderately coated BC particles should have few effects on our results presented in this study. The peak d_{me} value is identified as the mode value of a lognormal function that is fitted to the major peak of size distribution at each mobility.

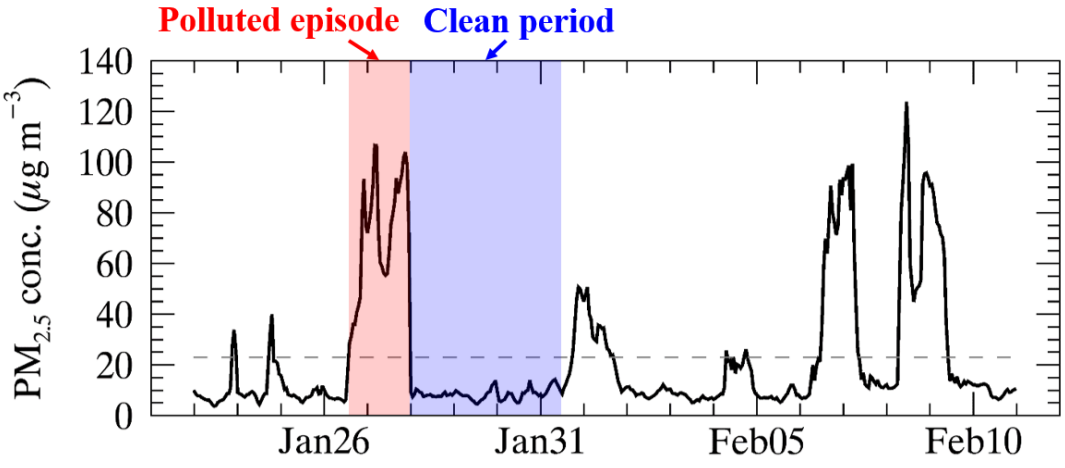

Fig. S7. Time series of hourly $PM_{2.5}$ mass concentrations measured at the same site during the experimental period. The dashed line represents the mean $PM_{2.5}$ mass concentration with a value of 23.0±26.7 μg m^{-3}. The red and blue shaded regions represent a polluted episode (mean $PM_{2.5}$=72.1±23.1 μg m^{-3}) and a consecutively clean period (mean $PM_{2.5}$=8.9±2.7 μg m^{-3}), respectively, in which the mass-mobility relationships of *ext*BC are compared.

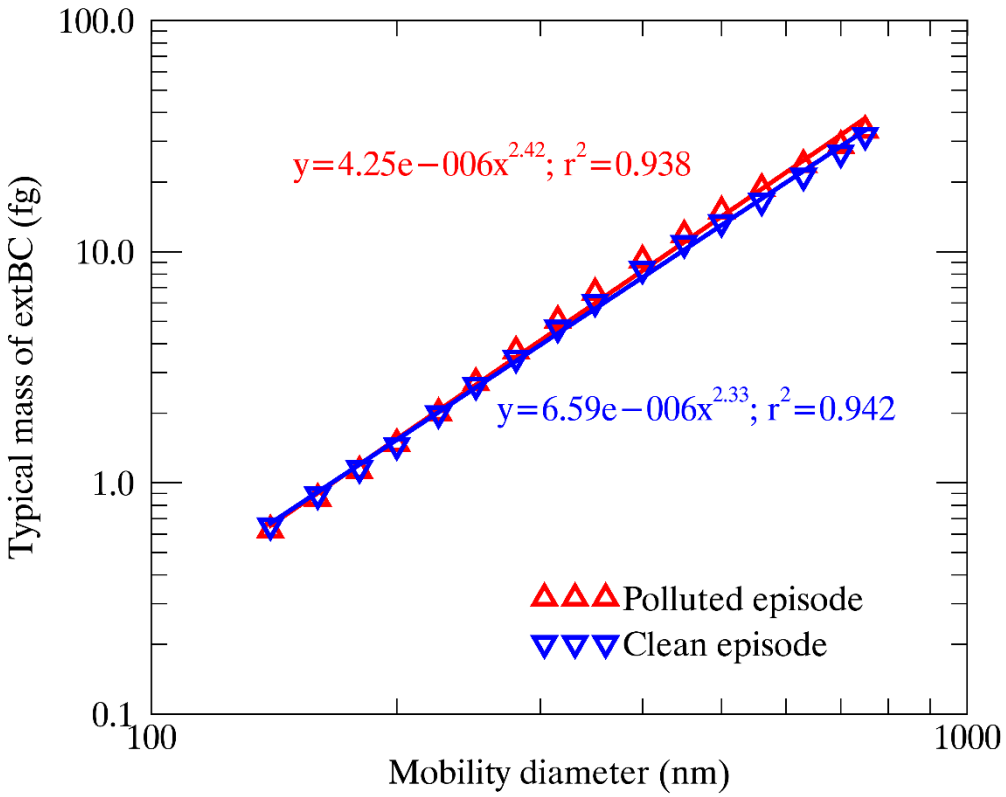

113

114 **Fig. S8.** The mass of *ext*BC particles as a function of the mobility diameter in the range of 140–
115 750 nm (black circles) in the polluted (red up-triangles) and clean (blue down-triangles) episodes.
116 The power-law functions are fitted to the mass-mobility relationships.

117

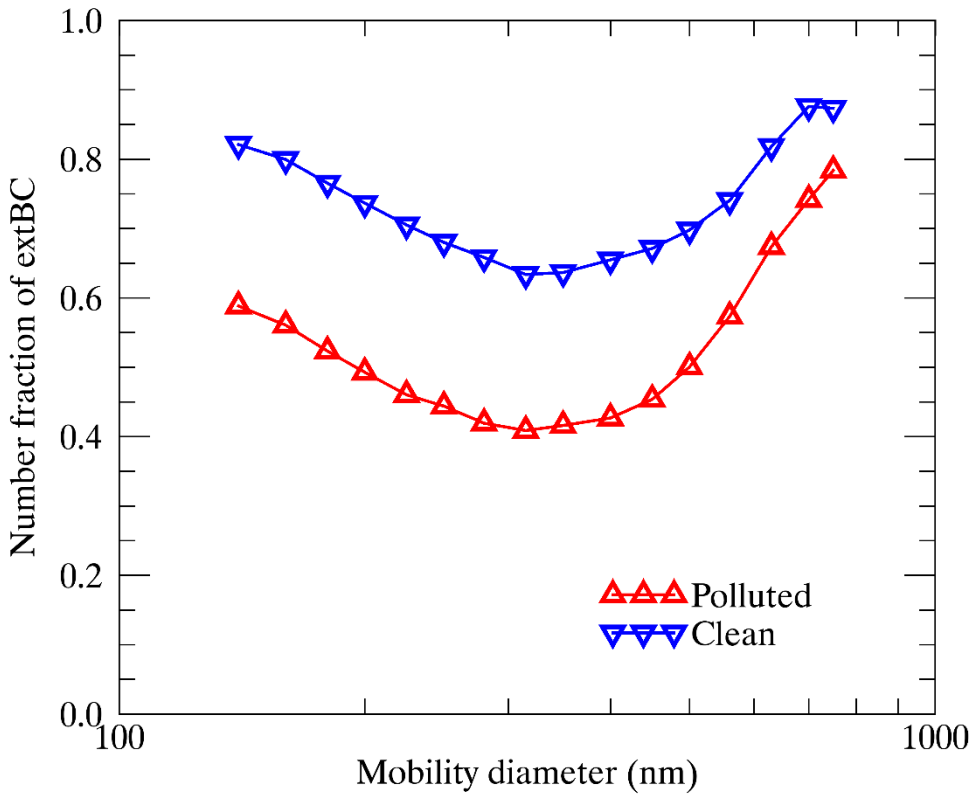

Fig. S9. The number fraction of *ext*BC as a function of the mobility diameter (d_{mob}) in the polluted episode (red up-triangles) and clean period (blue down-triangles). The fraction of *ext*BC is roughly calculated as the ratio of the *ext*BC number concentration to the sum of *ext*BC and internally mixed BC (*int*BC) particles at each d_{mob}. The effect of multicharged particles is not eliminated. However, the multicharged particles should result in a similar effect on *ext*BC and *int*BC at a given mobility. Thus, there should be few effects on the number fraction of *ext*BC. A detailed analysis of the mixing states of size-resolved BC particles will be performed in our future studies.

Table S1. The typical mass-equivalent diameters (d_{me}) and corresponding masses of *ext*BC at different mobility sizes (d_{mob}) selected by the DMA in the whole campaign. Three delay-time thresholds of 2.0, 1.2, and 0.4 μs are employed to discriminate *ext*BC.

d_{mob} (nm)	d_{me} (nm)			mass (fg)		
	t_{lag} < 2.0 μs	t_{lag} < 1.2 μs	t_{lag} < 0.4 μs	t_{lag} < 2.0 μs	t_{lag} < 1.2 μs	t_{lag} < 0.4 μs
140	88.8	88.4	86.7	0.66	0.65	0.61
160	97.5	97.6	96.2	0.87	0.88	0.84
180	106.2	106.6	105.0	1.13	1.14	1.09
200	115.6	116.2	114.2	1.46	1.48	1.40
225	127.9	128.8	125.8	1.97	2.01	1.88
250	140.5	141.6	138.1	2.62	2.67	2.48
280	155.8	156.9	152.9	3.56	3.64	3.37
315	172.6	173.6	169.4	4.85	4.93	4.58
350	188.2	189.2	184.7	6.28	6.38	5.94
400	207.4	208.6	204.8	8.41	8.55	8.10
450	226.4	228.0	224.1	10.94	11.17	10.61
500	243.8	245.4	241.2	13.65	13.92	13.23
560	262.6	265.4	262.0	17.06	17.62	16.96
630	283.2	286.1	285.3	21.42	22.07	21.88
700	305.1	307.9	309.8	26.76	27.52	28.03
750	319.6	322.3	323.4	30.76	31.57	31.87